Earth and Planetary Science Letters 301 (2011) 457–468

Contents lists available at ScienceDirect

Earth and Planetary Science Letters

journal homepage: www.elsevier.com/locate/epsl

Spatiotemporal patterns of fault slip rates across the Central Sierra Nevada frontal fault zone

Dylan H. Rood [a,b,*], Douglas W. Burbank [a], Robert C. Finkel [c,d]

[a] Department of Earth Science, University of California, Santa Barbara, CA 93106, USA
[b] Center for Accelerator Mass Spectrometry, Lawrence Livermore National Laboratory, Livermore, CA 94550, USA
[c] CEREGE, Aix en Provence, France
[d] Department of Earth and Planetary Science, University of California, Berkeley, CA 94720, USA

ARTICLE INFO

Article history:
Received 23 June 2010
Received in revised form 30 October 2010
Accepted 2 November 2010
Available online 15 December 2010

Editor: T.M. Harrison

Keywords:
fault slip rates
surface exposure dating
Be-10
Sierra Nevada
Walker Lane

ABSTRACT

Patterns in fault slip rates through time and space are examined across the transition from the Sierra Nevada to the Eastern California Shear Zone–Walker Lane belt. At each of four sites along the eastern Sierra Nevada frontal fault zone between 38 and 39° N latitude, geomorphic markers, such as glacial moraines and outwash terraces, are displaced by a suite of range-front normal faults. Using geomorphic mapping, surveying, and ^{10}Be surface exposure dating, mean fault slip rates are defined, and by utilizing markers of different ages (generally, ~20 ka and ~150 ka), rates through time and interactions among multiple faults are examined over 10^4–10^5 year timescales.

At each site for which data are available for the last ~150 ky, mean slip rates across the Sierra Nevada frontal fault zone have probably not varied by more than a factor of two over time spans equal to half of the total time interval (~20 ky and ~150 ky timescales): 0.3 ± 0.1 mm year^{-1} (mode and 95% CI) at both Buckeye Creek in the Bridgeport basin and Sonora Junction; and $0.4 + 0.3/-0.1$ mm year^{-1} along the West Fork of the Carson River at Woodfords. Data permit rates that are relatively constant over the time scales examined. In contrast, slip rates are highly variable in space over the last ~20 ky. Slip rates decrease by a factor of 3–5 northward over a distance of ~20 km between the northern Mono Basin ($1.3 + 0.6/-0.3$ mm year^{-1} at Lundy Canyon site) to the Bridgeport Basin (0.3 ± 0.1 mm year^{-1}). The 3-fold decrease in the slip rate on the Sierra Nevada frontal fault zone northward from Mono Basin is indicative of a change in the character of faulting north of the Mina Deflection as extension is transferred eastward onto normal faults between the Sierra Nevada and Walker Lane belt.

A compilation of regional deformation rates reveals that the spatial pattern of extension rates changes along strike of the Eastern California Shear Zone-Walker Lane belt. South of the Mina Deflection, extension is accommodated within a diffuse zone of normal and oblique faults, with extension rates increasing northward on the Fish Lake Valley fault. Where faults of the Eastern California Shear Zone terminate northward into the Mina Deflection, extension rates increase northward along the Sierra Nevada frontal fault zone to ~0.7 mm year^{-1} in northern Mono Basin. This spatial pattern suggests that extension is transferred from more easterly fault systems, e.g., Fish Lake Valley fault, and localized on the Sierra Nevada frontal fault zone as the Eastern California Shear Zone–Walker Lane belt faulting is transferred through the Mina Deflection.

1. Introduction

A deeper understanding of the temporal and spatial dynamics of faults and associated seismicity requires knowledge of the timing, rate, and spatial variation of tectonic processes that control the faulting. A fundamental assumption that underpins many crustal deformation models is that fault slip rates are steady once integrated across a sufficient number of seismic events. Short-term interseismic slip rates at regional scales are commonly assumed to be constant across time and space, and, therefore, they are used to predict long-term fault patterns. We know that this assumption may well be inaccurate on million-year time scales, but the assumption of steady rates remains largely untested at shorter time scales (Friedrich et al., 2003).

Few studies have assessed whether fault slip rates can change significantly at time scales ranging from 10^1 years to 10^5 years. With the maturing of geodetic sciences, our knowledge of decadal scale strain is rapidly improving. At large spatial scales (100 s of km), several studies deduce that geodetic rates are representative of long-term fault slip rates (Behr et al., 2010; Cowgill et al., 2009; DeCelles et

* Corresponding author. Center for Accelerator Mass Spectrometry, Lawrence Livermore National Laboratory, Livermore, CA 94550, USA. Tel.: +1 925 422 7378; fax: +1 925 423 7884.
E-mail address: rood5@llnl.gov (D.H. Rood).

0012-821X/$ – see front matter © 2010 Elsevier B.V. All rights reserved.
doi:10.1016/j.epsl.2010.11.006

al., 2002; Frankel et al., 2007a, 2007b; Ganev et al., 2009; Thompson et al., 2002; Wang et al., 2001) and match plate-motion rates (DeMets and Dixon, 1999; Dixon et al., 2000). At progressively smaller spatial scales and for shorter time intervals, data are lacking to assess whether the apparent constancy of long-term, large-scale rates can also be applied to these scales. If rates were constant, then geodetic measurements would represent snapshots of spatially variable strain fields that would provide a robust context for the interpretation of much Late Cenozoic geologic deformation in a given region (Thompson et al., 2002). In some sites, however, the currently defined geodetic and geologic rates are clearly not equivalent (Chevalier et al., 2005; Dixon et al., 2003; Oskin and Iriondo, 2004; Peltzer et al., 2001). Discrepancies between geodetic and geologic data that exist in the western US, e.g., Walker Lane belt, Wasatch Front, Owens Valley fault zone, Garlock fault, and Blackwater fault (Friedrich et al., 2003; Kirby et al., 2008; Lee et al., 2001; Oldow, 2003; Oskin et al., 2007, 2008) could result from clustering of past earthquakes (Rockwell et al., 2000) or geodetic sampling early in the interseismic cycle (Peltzer et al., 2001); they might reflect postseismic viscoelastic relaxation (Dixon et al., 2003); or they may be attributed to undetected or diffuse geologic deformation, e.g., Sheehan (2007).

Knowledge of the spatiotemporal patterns of deformation rates in a given region greatly assists efforts to reconstruct the behavior of a fault over time. Several recent studies have suggested that temporal clustering of earthquakes results in a punctuated record in which slip rates wax and wane, e.g., Rockwell et al. (2000), or cluster spatially. Data from southern California, for example, suggest that periods of clustered seismicity in the Eastern California Shear Zone (ECSZ) may alternate with clustered earthquakes in the Los Angeles basin (Dolan et al., 2007). Further, some geodetic data suggest that interseismic loading rates also vary, with more rapid loading during cluster intervals. Some detailed records indicate that slip rates over several earthquake cycles can actually exceed long-term plate slip rates (Weldon et al., 2004) or provide evidence for coordinated slip rate variations among neighboring faults (Kirby et al., 2006; Lee et al., 2009). Fault slip rates can accelerate and decelerate over glacial–interglacial cycles due to changes in surface loads, e.g., glacial ice or lakes (Hampel et al., 2007, 2009; Hetzel and Hampel, 2005). Variations in slip rates are also proposed as a result of interactions with volcanic systems, e.g., Hampel and Hetzel (2008). Moreover, emerging spatial patterns in fault slip rates in the ECSZ yield insights into fundamental processes of strain accommodation across tectonic boundaries, e.g., Frankel et al. (2007b), Ganev et al. (2009).

This paper evaluates the spatial and temporal patterns in fault slip rates across the central segment of the Sierra Nevada frontal fault zone (SNFFZ, Fig. 1) over the late Quaternary. This tectonic boundary is experiencing some of the highest strain rates and fastest Holocene slip rates in the western Great Basin (Hammond and Thatcher, 2004; Ramelli et al., 1999), yet the long-term slip rate history on these faults is poorly known. Better understanding of slip-rate variability across this fault system is critical for improved seismic hazard assessments and comparisons to contemporary geodetic data. We focus on time spans of 10^4–10^5 years and employ geomorphic mapping, geodetic surveying, and ^{10}Be surface exposure dating (Gosse and Phillips, 2001) to quantify rates of fault slip using multiple landforms as strain markers. Geomorphic markers are deposits, e.g., glacial moraines and outwash terraces, whose original morphology can be reconstructed across faults in order to estimate the magnitude of slip. At individual sites, these markers span several orders of magnitude of age range and, thus, allow us to test the variability (or consistency) of slip rates through time. With such data, we assess the time scales at which deformation is steady versus clustered or unsteady. Moreover, we compare slip histories at multiple sites with isochronous markers to identify spatial patterns in deformation rates. Finally, we synthesize our data with spatial patterns recognized elsewhere in the region to understand modes of strain accommodation across an important tectonic transition zone.

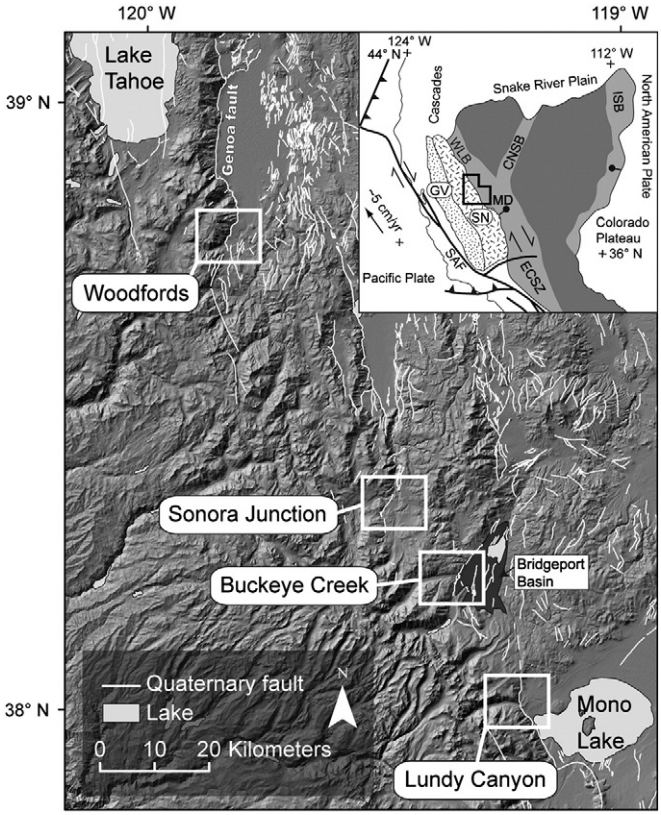

Fig. 1. Shaded relief image showing Quaternary faults (white) within the study area. Faults from the U.S. Geological Survey (USGS) Quaternary fault and fold database. Boxes (white) show location of slip-rate sites along the SNFFZ. (Inset) Simplified tectonic map of the western part of the U.S. Cordillera showing the major geotectonic provinces and modern plate boundaries; Basin and Range extensional province in dark gray, CNSZ (central Nevada seismic zone), ECSZ (eastern California shear zone), ISB (intermountain seismic belt), and WLB (Walker Lane belt) in light gray. Box (black) shows location of study area along the Sierra Nevada frontal fault zone (SNFFZ) (modified after Glazner et al., 2005). GV = Great Valley, SN = Sierra Nevada, SAF = San Andreas Fault, MD = Mina Deflection.

1.1. Regional tectonic setting

Up to 25% of the plate boundary deformation in the western US is currently localized within a ~100–150 km wide dextral shear zone referred to as the Eastern California Shear Zone (ECSZ) and Walker Lane belt (WLB). The ECSZ-WLB (Wesnousky, 2005a) is defined by a belt of active seismicity that trends from the Gulf of California, through the Mojave Desert, and along the western edge of the Great Basin (Fig. 1). Focusing of deformation near the western edge of the Great Basin is suggested by Quaternary fault patterns (Dokka and Travis, 1990; Wallace, 1987), seismicity (Eddington et al., 1987; Oldow, 2003), and geodesy (Bennett et al., 1998; Dixon et al., 1995, 2000; Hammond and Thatcher, 2004; Thatcher et al., 1999). The Sierra Nevada frontal fault zone (SNFFZ) is the normal fault system located on the westernmost margin of the Great Basin at the tectonic boundary between the relatively undeformed Sierra Nevada–Great Valley block and WLB (Fig. 1). Geodetic surveys and elastic block models suggest that the motion of the rigid Sierra Nevada block with respect to North America is ~9–10 mm year^{-1} toward the NW (~N25°W at 37–38° N latitude), oblique to the strike of the SNFFZ and ECSZ-WLB (Bennett et al., 2003; Dokka and Travis, 1990; Sauber et al., 1994; Savage et al., 1990, 2001). Kinematic inversions of earthquake focal mechanisms (Unruh et al., 2003) suggest the Sierra Nevada–Walker Lane transition is a zone of active transtensional deformation, with GPS data suggesting ~1 mm year^{-1} of extension across a broad

zone east of the Sierra Nevada (Bennett et al., 2003). At ~38° N latitude, the dextral and oblique faults of the ECSZ-southern WLB step to the east across the Mina Deflection (Fig. 1) and transfer slip to faults of the central WLB. The Mina Deflection is characterized by ENE- and NE-striking left-lateral faults that accommodate clockwise vertical-axis block rotations (Petronis et al., 2002; Wesnousky, 2005b). The role that the SNFFZ has in accommodating extension in this transfer zone, however, remains unclear. North of the Mina Deflection, faulting is again partitioned between normal and dextral fault systems (Cashman and Fontaine, 2000; Oldow et al., 2001; Surpless, 2008). In the central western Great Basin at 38–39° N latitude (Fig. 1), the transition from the Sierra Nevada to the Walker Lane consists of a series of left-stepping *en echelon* escarpments and fault-bounded basins that reflect normal faulting, including faults of the SNFFZ (Schweickert et al., 2004; Wakabayashi and Sawyer, 2001).

1.2. Previous work

Several previous studies address the Quaternary fault slip rates on some of the normal faults of the SNFFZ. Whereas offsets of glacial and alluvial markers across the range-front fault system have been documented in many sites, the resolution of their slip rate calculations has been limited by their dating methods, e.g., Bursik and Sieh (1989), Martel et al. (1987). Studies at 37–38° N latitude suggest that dip-slip rates (from south to north) are 0.5 ± 0.2 mm year^{-1} on the Lone Pine fault (Lubetkin and Clark, 1988), 0.2–0.3 mm year^{-1} on the southern SNFFZ (Le et al., 2007), 0.2 ± 0.1 mm year^{-1} on the Fish Springs fault (Zehfuss et al., 2001), and 0.4 ± 0.1 mm year^{-1} on the Round Valley fault and 0.9 ± 0.2 mm year^{-1} on the Hilton Creek fault (Berry, 1997). Studies across a transect in the northern Owens Valley suggests slip rates of ~1.0 mm year^{-1} on the frontal fault near Tinemaha and Birch Creeks, 0.2–0.3 mm year^{-1} for the Red Mountain fault, and ~0.2 mm year^{-1} in Waucobi embayment (Greene et al., 2007). Kent et al. (2005) first used seismic imaging of faults in Lake Tahoe with radiocarbon and OSL dates from core samples to calculate a cumulative slip rate of 0.9 ± 0.2 mm year^{-1} across the basin, and Brothers et al. (2009) used similar methods to estimate a slip rate of 0.4–0.8 mm year^{-1} on the West Tahoe–Dollar Point fault. Only two published studies use modern surface exposure dating methods; Le et al. (2007) and Zehfuss et al. (2001) applied ^{10}Be dating methods to faulted alluvial fans in the northern and central Owens Valley, respectively. These studies from individual basins permit a view of the spatial and temporal patterns of fault slip along the northern and southern segments of the eastern Sierra Nevada. Focused on the central segment of the eastern range front, our study increases the number of high-resolution slip rate estimates along the SNFFZ, provides tests of the steadiness of slip rates over the past ~20 ky and ~150 ky, and, together with the previous work, allows for spatial and temporal patterns in fault slip rates to be resolved and interpreted in a regional tectonic context.

2. Methods

We use surface mapping, topographic survey profiling, and ^{10}Be surface exposure dating with Monte Carlo simulations (Fig. 2) to define the location, geometry, magnitude, and rates of late Quaternary faulting across the SNFFZ. Comparisons of multiple offset features enable us to examine: 1) whether statistically significant changes in rates occur and 2) how much uncertainty should be incorporated into slip rate estimates (combinations of age and geometric uncertainties, Fig. 2). Most of the displacement rates are derived from a four-step process: i) geomorphic mapping (Fig. 3); ii) topographic surveying of faulted features, such as outwash surfaces and moraine crests (Figs. 2 and 3); iii) dating of these displaced Quaternary deposits as measured using ^{10}Be surface exposure dating; and (iv) Monte Carlo simulations of slip rates. Wherever two or more markers of different ages are cut by the same fault, we obtain average rates for each marker and perhaps more informatively, interval rates between pairs of markers.

2.1. Mapping

We used local Quaternary deposits (glacial outwash terraces and moraines) as geomorphic strain markers to reconstruct the rate of fault slip since the late and middle Pleistocene at each site along the SNFFZ. We selected study sites in order to maximize the following elements: (1) areas with several, well-exposed/well-preserved geomorphic markers; (2) markers of different ages with a broad spatial extent; (3) multiple Quaternary markers differentially offset by the same faults; and (4) planar or linear markers for calculating vertical offsets across normal faults, e.g., terrace treads or moraine crests. We focus on four areas where a concentration of offset features exists: Lundy Canyon in the northern Mono Basin, Buckeye Creek in the Bridgeport basin, Sonora Junction near Sonora Pass, and Woodfords along the West Fork of the Carson River (Fig. 1).

Following the previous work of Bursik (1989), Clark (1967), Ramelli et al. (1999) and Sharp (1972), we mapped glacial moraines, outwash terraces, and fault scarps at these four sites (Fig. 1). Geomorphic mapping was completed on aerial photographs, then orthorectified and digitized in ESRI ArcGIS. The typical Sierran glacial nomenclature (Tioga, Tenaya, Tahoe, Mono Basin, Sherwin: Sharp, 1972) used by previous authors was retained for simplicity. The glacial moraines and outwash terraces on which we focused our chronologic and survey efforts were selected for their level of preservation and clear fault offsets.

2.2. ^{10}Be dating

^{10}Be surface exposure dating results are discussed in detail in Rood et al. (2010), including sampling, chemistry, analytical results, and age calculations. We include here (i) the locations of sampled surface boulders and a depth profile (Fig. 3) and (ii) interpreted best-estimate ages for each of the markers that is included in our analysis (Tables 1 and S2). When suitable materials were available, samples were collected from both the hangingwall and footwall of each fault offset to validate the correlation of each deposit across the fault. Only markers with high- or moderate-confidence ages were included in the analysis, except for the Tahoe outwash terrace at Woodfords where an average age for coeval terraces is used (discussed further in Section 3.4). Overall, the 115 new ^{10}Be dates from this study fall into two main subsets: Tioga-aged features dating from 19 ± 2 ka and Tahoe-aged features dating from 144 ± 14 ka (Rood et al., 2010).

2.3. Surveying

Most fault scarps and offsets of geomorphic markers were surveyed using a Trimble 4700 differential GPS (dGPS) with centimeter-scale vertical and horizontal precision. At sites where vegetation cover precluded using dGPS, survey data were collected using a Leica TC805-L total station. At the Woodfords site (Figs. 1 and 3), topographic profiles were supplemented by extracting elevation data from the 30-m SRTM digital elevation model (DEM). Surveying focused on scarps in well-preserved terrace treads and moraine crests that appeared to have experienced minimal modification or scarp erosion. For each offset, at least 2 (max. of 4) topographic profiles were measured approximately perpendicular to the surface fault trace (Fig. 3). One of the potentially confounding factors in such a study is that displacements and ages are typically calculated at a given point on a fault, and then these slip values are assigned to the entire fault. This generalization of slip rates tends to ignore the potential complexity of along-strike variability in slip. In the study sites, fault scarps can be traced extensively along outwash surfaces and across multiple nearby moraines, often apparently belonging to the same

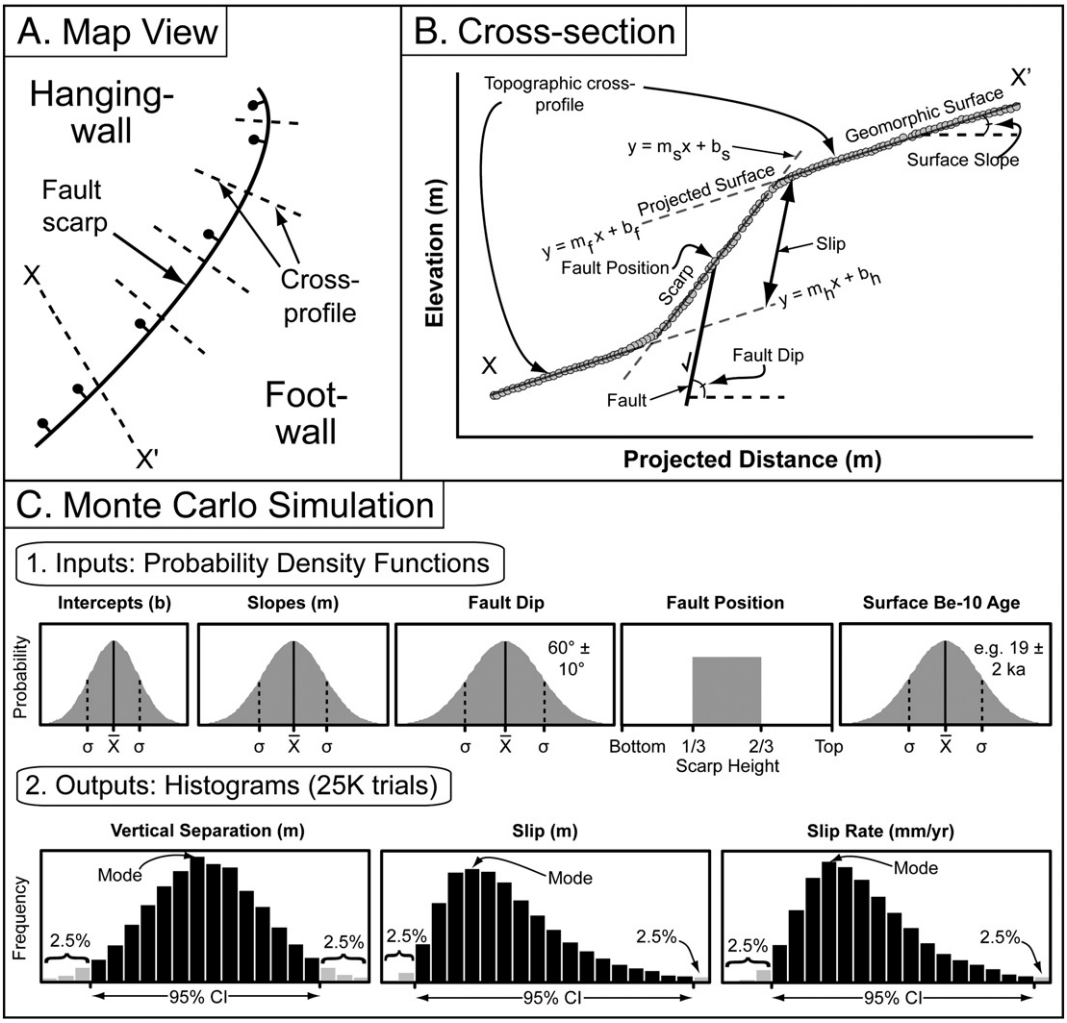

Fig. 2. Diagram depicting procedures and calculations of displacement associated with each normal fault. (A) Schematic map showing trace of normal fault scarp (solid black line with ball on downthrown side) and survey profiles (dashed black line). X–X′ indicates orientation of cross-section in (B). (B) Parameters measured from the survey cross-profile and estimated from other faults, such as fault dip and fault position. (C) Five parameters and associated uncertainties are combined in a Monte Carlo simulation to provide the best estimate of magnitude and rate of fault slip.

glaciation. Through surveying along these scarps and comparison of features of equivalent age, we exploit these markers to define along-strike variability (if any) in slip magnitude and rates. When possible, multiple profiles were used to test for reproducibility of slip rate results. Only relatively simple offsets with high- or moderate-confidence dating results were included in our analysis.

2.4. Monte Carlo simulation

The sage-dominated slopes of the lower eastern Sierra Nevada and western Great Basin permit ready surveying of most landforms, such that the major uncertainties in the magnitude of structural offsets derive from the standard challenges of defining how landforms project across various faults. Following the approach of Amos et al. (2007), Davis et al. (2005) and Thompson et al. (2002), we calculate slip rates and their uncertainties by applying Monte Carlo simulations that enable us to incorporate uncertainty estimates for ages, surface slopes, fault dips, projections of displaced features, and fault position along scarps (Fig. 2). Monte Carlo simulations were done using Oracle Crystal Ball, a worksheet-based software package designed for predictive modeling.

In the Monte Carlo simulations, each input is assigned a probability density function (PDF) that best describes the uncertainty on that variable (Fig. 2), similar to the approach of Zechar and Frankel (2009). The slope of the offset geomorphic feature (and its projection) is estimated using a least-squares linear regression fit to topographic survey points. The regression assumes a normal distribution of the scatter in the data about the line. Thus, for geometric inputs that are approximated by a linear regression, i.e., slope and intercept, a PDF with a normal distribution (defined by the mean and standard deviation) is assigned to the variable. A normal distribution is also used to estimate the errors on the fault dip, which is assumed to be 60 ± 10° based on data for normal faults in the western Great Basin (Table S1 in supplemental material). Errors on the surface age are generally described by a normal distribution using the average and standard deviation of surface boulders (Rood et al., 2010; Table 1). Furthermore,

Fig. 3. Geologic maps showing offset Quaternary moraines and outwash terraces at the (A) Lundy Canyon (LC) site in Mono Basin (modified after Bursik, 1989), (B) Buckeye Creek (BC) site in Bridgeport Basin (modified after Sharp, 1972), (C) Sonora Junction (SJ) site near Sonora Pass (modified after Clark, 1967), and (D) Woodfords site on the southern Genoa fault (modified after Ramelli et al., 1999) (locations on Fig. 1). Survey line numbers correspond to individual profiles in the supplementary data. Circles depict location of boulders sampled for ^{10}Be dating. Individual exposure ages in ky (Table S2).

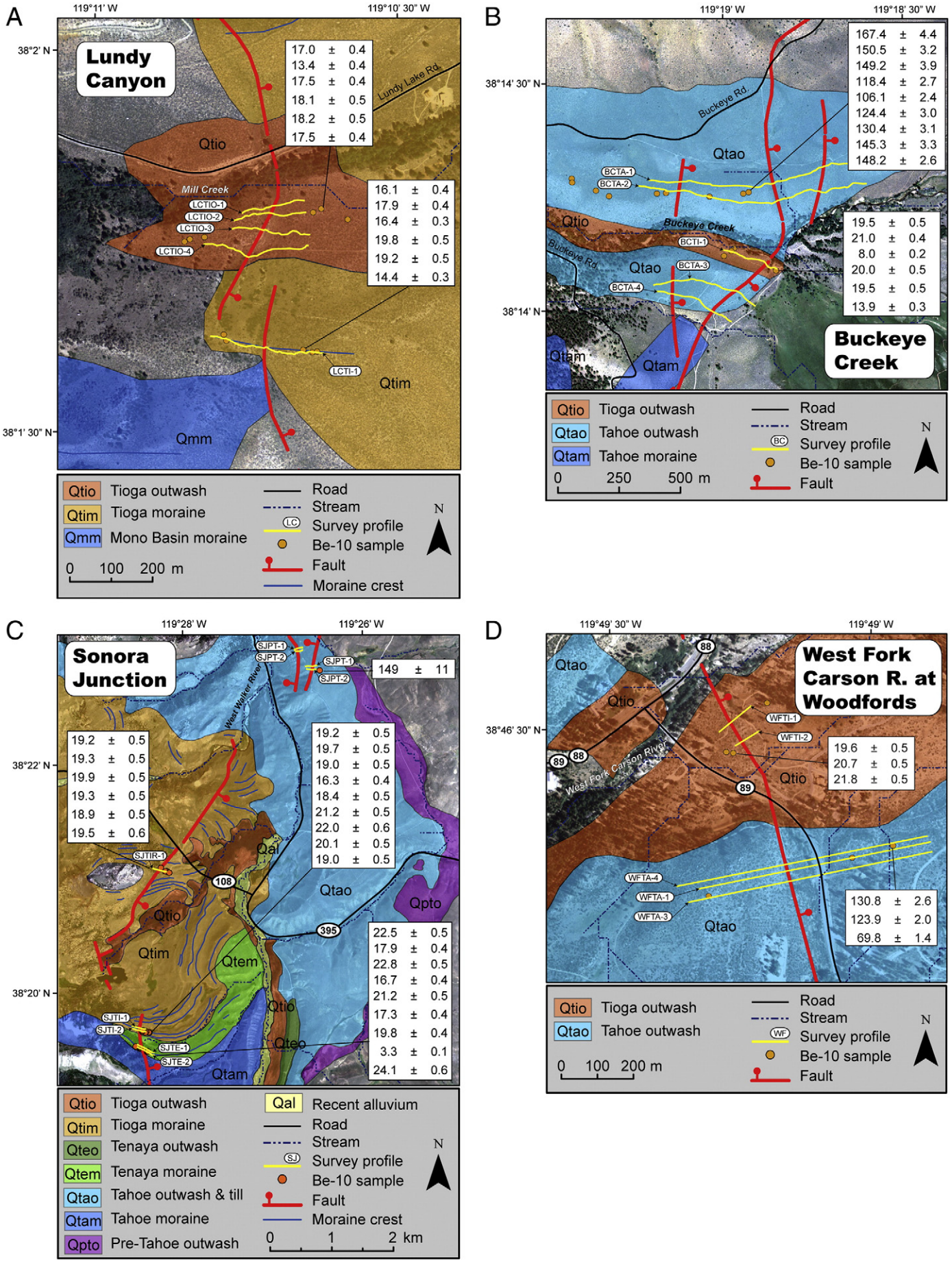

Table 1
Summary of fault slip rates from Monte Carlo simulations of scarp profiles and ^{10}Be surface exposure ages.

Profile	Survey method[a]	Slip mode (m)	Slip uncertainty (m) (95%CI)	Age association[b]	Exposure age (ky)	Age uncertainty (ky) (1σ)[c]	n[d]	Slip rate mode (mm year^{-1})	Slip rate uncertainty (mm year^{-1}) (95%CI)
Sonora Junction Tioga moraines									
SJTI-1	dGPS	7	+3/−1	SJTI05	19	+/−1	6	0.4	+0.2/−0.1
SJTI-2	dGPS	5	+2/−1	SJTI05	19	+/−1	6	0.3	+0.1/−0.1
SJTIR-1	Total station	6	+3/−1	SJTI06	19	+/−1	6	0.3	+0.1/−0.1
Sonora Junction Tenaya moraine									
SJTE-1	dGPS	9	+4/−1	SJTE06	20	+/−3	8	0.4	+0.3/−0.1
SJTE-2	dGPS	8	+3/−1	SJTE06	20	+/−3	8	0.4	+0.2/−0.1
Sonora Junction Tahoe outwash terrace									
SJPT-1	dGPS	42	+8/−5	SJPT06	149	+/−11	9	0.3	+0.1/−0.1
SJPT-2	dGPS	51	+12/−6	SJPT06	149	+/−11	9	0.4	+0.1/−0.1
Buckeye Creek Tioga outwash terrace									
BCTI-1	dGPS	6	+2/−1	BCTI07	20	+/−1	4	0.3	+0.1/−0.1
Buckeye Creek Tahoe outwash terrace									
BCTA-1	dGPS	45	+13/−10	BCTA06	148	+/−2	4	0.3	+0.1/−0.1
BCTA-2	dGPS	48	+12/−9	BCTA06	148	+/−2	4	0.3	+0.1/−0.1
BCTA-3	dGPS	44	+14/−6	BCTA06	148	+/−2	4	0.3	+0.1/−0.1
BCTA-4	dGPS	44	+15/−8	BCTA06	148	+/−2	4	0.3	+0.1/−0.1
Lundy Canyon Tioga outwash terrace									
LCTIO-1	dGPS	23	+9/−2	LCTIO-07	18	+/−1	5	1.3	+0.6/−0.2
LCTIO-2	dGPS	23	+9/−2	LCTIO-07	18	+/−1	5	1.3	+0.6/−0.2
LCTIO-3	dGPS	24	+10/−2	LCTIO-07	18	+/−1	5	1.4	+0.5/−0.2
LCTIO-4	dGPS	22	+10/−2	LCTIO-07	18	+/−1	5	1.2	+0.6/−0.2
Lundy Canyon Tioga moraine									
LCTI-1	dGPS	22	+7/−2	LCTI07	18	+/−2	5	1.2	+0.5/−0.2
Woodfords Tioga outwash terrace									
WFTI-1	Total station	10	+5/−2	WFTI08	20	+/−1	3	0.5	+0.2/−0.1
WFTI-2	Total station	94	+4/−1	WFTI08	20	+/−1	3	0.4	+0.2/−0.1
Woodfords Tahoe outwash terrace									
WFTA-1	SRTM	59	+21/−9	SJPT06/BCTA06	150	+9/−12	13	0.4	+0.2/−0.1
WFTA-3	SRTM	42	+20/−10	SJPT06/BCTA06	150	+9/−12	13	0.3	+0.2/−0.1
WFTA-4	SRTM	66	+23/−8	SJPT06/BCTA06	150	+9/−12	13	0.4	+0.2/−0.1

[a] Topographic survey data derived from differential GPS (dGPS), total station, or SRTM 30-m digital elevation model.
[b] Best-estimate depositional ages from Rood et al. (2010). Woodfords Tahoe outwash terrace uses an average age for SJPT06 and BCTA06 (see text for details).
[c] Uncertainty for SJPT06/BCTA06 is 95% confidence interval on average age from Monte Carlo simulation results.
[d] Number of samples on which each depositional age is based (see Table S2 for individual ages.)

the position of the fault on the scarp is assumed to be near the middle of the scarp, consistent with paleoseismic trenching and scarp diffusion modeling of normal faults in the Great Basin (Table S1). Thus, we use a boxcar PDF that assigns an equal likelihood that the fault occurs between one-third and two-thirds of the scarp height (Fig. 2).

The outputs of the Monte Carlo simulations reported here rely on the input parameters defined above (Fig. 2) and result from 25,000 trial runs in which each individual calculation is computed by randomly drawing values from each input variable based on the assigned PDF. A histogram showing the frequency of predicted values is used to define the mode and 95% confidence interval for vertical separation, total slip, and average slip rate. The histograms are made with the maximum number of bins while maintaining a clear modal value. In places where multiple parallel fault strands cut a single feature, an additional Monte Carlo simulation is used to sum the individual scarp offsets using the total slip histogram for each strand as an input. Combined with the surface age and error, this simulation generates an output for the total slip rate across the fault zone.

Interval slip rates between two nearby markers of different ages are also calculated using Monte Carlo simulations. The output total slip histogram for each marker and the PDF of each marker's age are used as inputs and differenced. By iteratively sampling from these inputs, a histogram of interval slip and interval time is generated. An additional Monte Carlo simulation is run in the same way to generate an output histogram that defines the mode and 95% confidence limits on the slip rate between pairs of markers.

3. Results

A representative cross-profile and slip rate calculation from Lundy Canyon illustrates the typical uncertainties resulting from the Monte Carlo simulations (Fig. 4). Results for each individual scarp profile and its Monte Carlo outputs for slip rate calculations are presented in the supplemental materials (Figs. S1–21). The results of 22 slip rate calculations from the four study sites, including estimated total slip, age, and slip rate with associated uncertainties (Table 1) and changes in rates through time (Table 2) serve to define spatiotemporal patterns of fault slip rates in the central Sierra Nevada front fault system. Below we describe key site characteristics and the results from each study site (from south to north, Fig. 1).

3.1. Lundy Canyon

In the northern Mono Basin at the Lundy Canyon site, the late Pleistocene slip-rate of ~1.3 mm year^{-1} (Table 1) is the highest in the region. Clear offsets of moraines and an outwash terrace of the Tioga glaciation are present along Mill Creek (Fig. 3A). Fault scarps can be recognized for their fresh morphology and abundant spring discharge

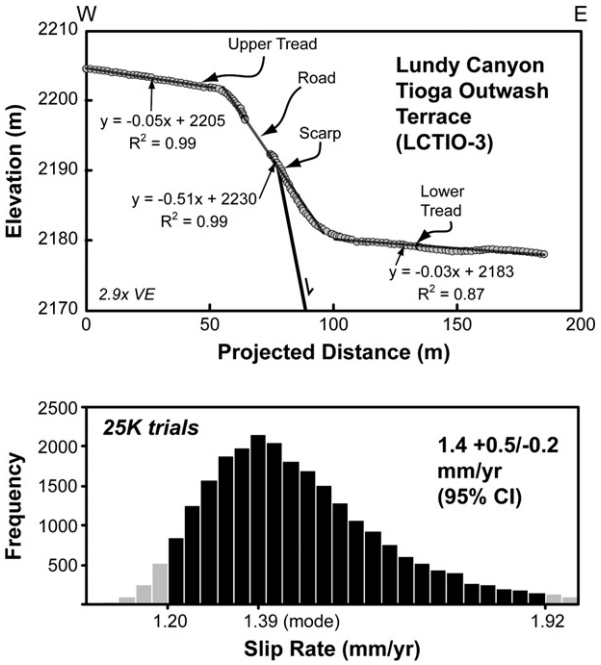

Fig. 4. Example calculations of displacement associated with a Tioga outwash terrace at Lundy Canyon offset across a normal fault using parameters measured from the survey profile (upper) and Monte Carlo simulation output (lower) that gives the slip rate and 95% confidence intervals. See Figure 2 for inputs to the Monte Carlo simulation. Profiles and Monte Carlo outputs for each individual scarp are included in the supplemental materials.

(and associated vegetation lineaments) (Fig. 5). Older glacial deposits topographically above and outside of the right-lateral Tioga moraines are clearly truncated across the range-front fault (Fig. 5) and form triangular-faceted hillslopes. These older moraines are mapped as equivalent to deposits of the Mono Basin and Sherwin glaciations (Bursik and Sieh, 1989), and provide minima for the dip-slip displacement across the fault with large uncertainties. The burial of these older moraines on the hangingwall side of the fault, however, supports the high rates of slip calculated on this range-front fault.

Six boulders for ^{10}Be dating were collected from each of two offset Tioga deposits. The Tioga moraine gives a best-estimate age of 17.9 ± 1.6 ka (n = 5) (Rood et al., 2010; Table 2). The survey profile along the moraine crest indicates total slip of 22 +7/−2 m (Fig. S1) and a slip rate of 1.2 +0.5/−0.2 mm year^{-1} (Table 1). The Tioga outwash terrace produced a ^{10}Be age of 17.7 ± 1.0 ka (n = 5). Four topographic profiles of scarps in the terrace tread give total slip estimates of 23 +9/−2, 23 +9/−2, 24 +10/−2, and 22 +10/−2 m and slip rates of 1.3 +0.6/−0.2, 1.3 +0.6/−0.2, 1.4 +0.5/−0.2, 1.2 +0.6/−0.2 mm year^{-1}, respectively (Table 2; Figs. 4 and S2–S4). The agreement among the slip rate estimates for the coeval moraine and outwash terrace and the reproducibility of results along strike suggest a robust slip-rate determination at this site. An interval rate could not be calculated at Lundy Canyon because the older deposits are not preserved on the hangingwall of the fault.

3.2. Buckeye Creek

Bridgeport Basin (Buckeye Creek site, Fig. 3) shows a well-preserved record of Quaternary faulting. The elevation of the basin floor is ~1970 m, significantly higher than valleys in a comparable position to the north and south (Clark et al., 2003). Due to the low gradient and high elevation of the valley, Pleistocene glaciers with snowlines similar to those of other Sierra Nevada glaciers (Kessler et al., 2006) flowed far into the basin and are exceptionally well-preserved where they cross the basin-bounding faults. Sharp (1972) mapped the distribution of glacial deposits of at least five different ages, which are some of the most well-preserved glacial deposits in the eastern Sierra Nevada. Quaternary deposits of at least 2 different ages are cut by the same fault system, including fresh 1–2 m Late Holocene scarps (Fig. 5).

Along strike of the basin-bounding fault system, an outwash terrace of the Tahoe glaciation and an outwash terrace of the Tioga glaciation are differentially offset by the same fault system (Fig. 3). Survey data across well-preserved terrace treads reveal one to three scarps. 6–10 boulder samples for ^{10}Be dating were collected from the surface of each terrace. Samples from the faulted Tahoe outwash terrace give a ^{10}Be age of 148.3 ± 2.2 ka (n = 4) (Table 1). Survey data yield cumulative dip slip magnitudes of 45 +13/−10, 48 +12/−9, 44 +14/−6, and 44 +15/−8 m (Figs. S5–S8), and yield a dip-slip rate of 0.3 ± 0.1 mm year^{-1} for this normal fault system associated with the SNFFZ. Although the number of scarps and scarp heights in the Tahoe terrace changes along strike, the total slip (and slip rate) remains rather constant. The Tioga outwash terrace gave a best-estimate ^{10}Be age of 20.0 ± 0.7 ka (n = 4), a calculated slip estimate of 6 +2/−1 m (Fig. S9), and a slip rate of 0.3 ± 0.1 mm year^{-1}. Furthermore, the difference in the age and magnitude of offset of the two terraces yields an interval rate of 0.3 ± 0.1 mm year^{-1} between 20 and 140 ka (Table 2). These results permit that slip rates along this segment of the SNFFZ are relatively constant over ~20 ky and ~150 ky timescales, and have probably not varied by more than a factor of two.

3.3. Sonora Junction

Mapping in the Sonora Pass region (Fig. 3) reveals an extensive record of Sierra Nevada range-front faulting. The largest Pleistocene glaciers of the eastern slope of the Sierra Nevada occupied the West

Table 2
Interval fault slip rates from Monte Carlo simulation results.

Best-estimate scarp profiles		Interval slip mode (m)	Interval uncertainty (m) (95% CI)	Age association[a] (Tahoe to Tioga)	Interval time mode (ky)	Interval time uncertainty (ky) (95% CI)	Interval slip rate mode (mm year^{-1})	Interval slip rate uncertainty (mm year^{-1}) (95% CI)
Older (~150 ka) (Tahoe)	Younger (~20 ka) (Tioga)							
Sonora Junction								
SJPT-1	SJTI-1	34	+9/−4	SJPT06-SJTI05	126	+23/−19	0.3	+/−0.1
SJPT-1	SJTE-1[b]	32	+9/−4	SJPT06-SJTE06	128	+21/−21	0.3	+/−0.1
SJPT-1	SJTIR-1	36	+8/−5	SJPT06-SJTIR05	127	+22/−19	0.3	+/−0.1
Buckeye Creek								
BCTA-2	BCTI-1	41	+12/−9	BCTA06-BCTI06	128	+25/−4	0.3	+/−0.1
Woodfords								
WFTA-1	WFTI-1	47	+20/−8	SJPT06/BCTA06-WFTI08[c]	130	+9/−12	0.4	+/−0.1

[a] Same as in Table 1.
[b] Tenaya moraine with age similar to Tioga.
[c] Tahoe age assigned from terraces at Sonora Junction and Buckeye creek.

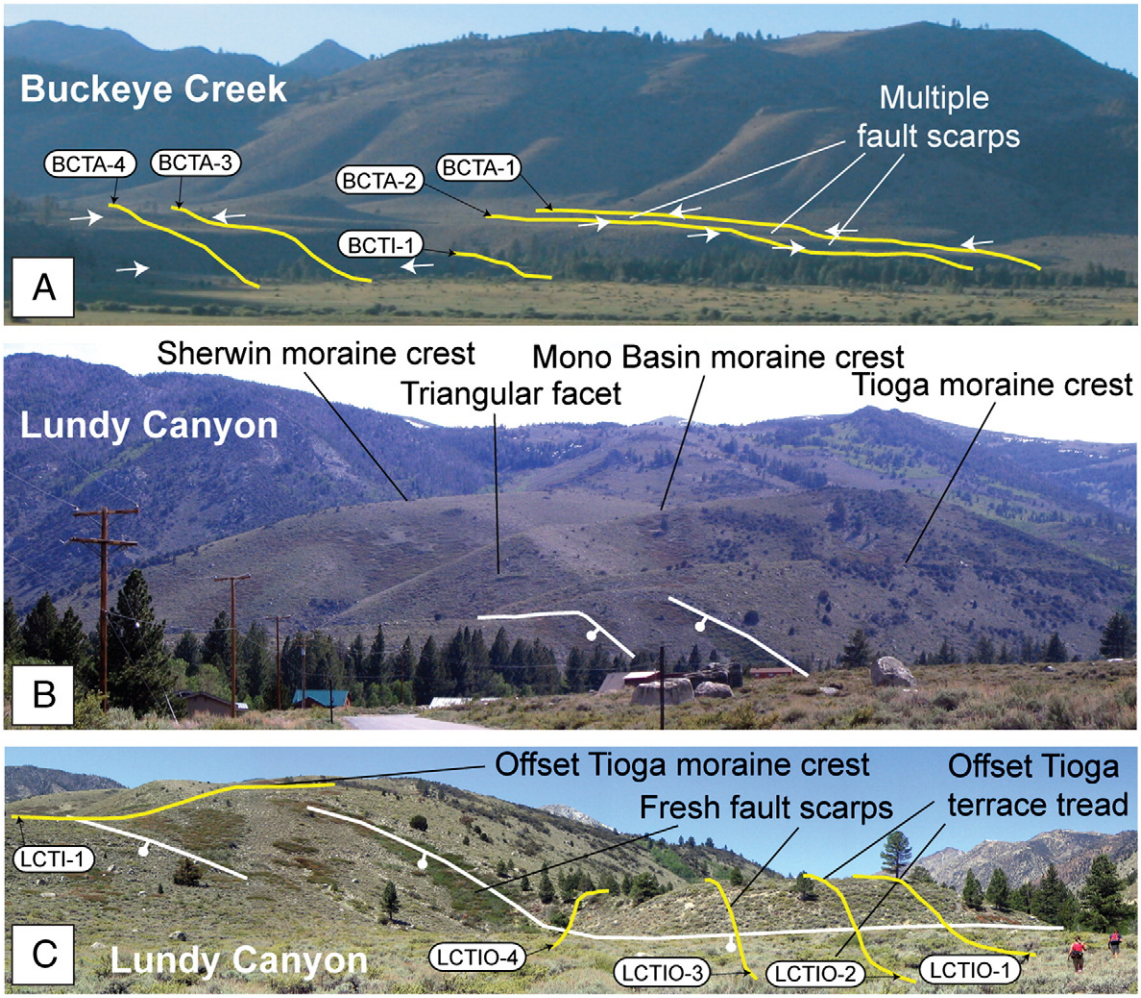

Fig. 5. (A) Field photo (view to NW) of Buckeye Creek site showing labeled differential GPS survey profiles across multiple fault scarps cutting outwash terraces of the Tahoe and Tioga glaciations. (B) View toward southwest of Sierra Nevada range-front in northern Mono Basin at Lundy Canyon showing normal faults right-lateral moraine crests of three different glacial stages. Note triangular facets of older moraine crests along the fault and offset of Tioga moraine crest. (C) View toward west of labeled survey profiles and fault scarps cutting Tioga moraine and outwash terraces at Lundy Canyon. Note springs and vegetation lineaments along fault trace.

Walker River drainage near Sonora Pass. Previous work in the region indicates that at least five suites of glacial deposits are present, the oldest of which is mantled with a volcanic ash dated at ~550 ka, whereas the youngest deposits are Tioga moraines (Clark et al., 2003). A right-stepping normal fault of the SNFFZ differentially offsets Quaternary deposits of at least 2 different ages (mapped as Tahoe, Tenaya, and Tioga deposits).

Survey data revealed two W-facing scarps in the Tahoe outwash terrace (Fig. S10), from which a depth profile was collected for dating based on the method of Anderson et al. (1996) using sediment samples beneath the well-preserved tread. East-dipping fault scarps along crests of one Tenaya and two Tioga moraines serve to quantify the fault slip rate at three different locations along strike for the same Quaternary time interval (Table 1). 6–10 samples for ^{10}Be geochronology were collected from boulders on a moraine of each age. Subsequent analyses define two average deformation rates throughout Quaternary time and allow calculation of the interval rate between Tioga and Tahoe deposits.

The depth profile from the Tahoe outwash terrace gives an age of 149.1 ± 10.5 ka (Rood et al., 2010; Table 1). The two fault scarps offsetting the tread give an estimated summed slip of 42 +8/−5 and 51 +12/−6 m (Figs. S10–S11) and slip rates of 0.3 ± 0.1 and 0.4 ± 0.1 mm year^{-1}, respectively. 6–9 samples for ^{10}Be dating were processed and analyzed from boulders on the faulted Tenaya and Tioga moraines. The Tenaya moraine gives a ^{10}Be age of 20.3 ± 2.8 ka (n = 8) and offsets from two surveys along the Tenaya moraine crest give calculated slip of 9 +4/−1 and 8 +3/−1 m (Figs. S12–S13) and a slip rate of 0.4 +0.3/−0.1 and 0.4 +0.2/−0.1 mm year^{-1} (Table 1). The Tioga moraine associated with the southern ice lobe gives a best-estimate age of 19.2 ± 0.6 ka (n = 6). Profiles along the moraine crest give slip estimates of 7 +3/−1 and 5 +2/−1 m (Figs. S14–S15) and slip rates of 0.4 +0.2/−0.1 and 0.3 ± 0.1 mm year^{-1}, respectively. Samples from another right-lateral Tioga moraine (northern lobe) yield an age of 19.4 ± 0.3 ka (n = 6) (Table 1). A survey of the offset moraine crest gives a dip-slip estimate of 6 +3/−1 m (Fig. S16) and a slip rate of 0.3 ± 0.1 mm year^{-1}. Combining all these data, Monte Carlo simulation results suggest that the interval slip rate is also 0.3 ± 0.1 mm year^{-1} (Table 2). Together these data suggest that the average slip rate across the fault zone has probably not varied by more than a factor of two over time spans equal to half of the total time intervals (~20 ky and ~150 ky), consistent with results from the Buckeye Creek site.

3.4. West Fork Carson River at Woodfords

The Woodfords site provides a relatively complete record of faulting across the southern Genoa fault (Fig. 3). Pleistocene glaciers of the eastern slope of the Sierra Nevada occupied Hope Valley (upper West Carson River drainage near Carson Pass) and terminated near

Woodfords (Armin and John, 1983). The Genoa fault differentially offsets Quaternary deposits of multiple ages, including outwash and a moraine of the Tahoe glaciation and outwash of the Tioga glaciation, younger alluvial fans, and a Holocene terrace (Ramelli et al., 1999). Profiles (Fig. 4) were analyzed across fault scarps on both outwash surfaces in order to quantify fault slip rates over different Quaternary time intervals. Total station survey data was collected across fault scarps on the Tioga outwash surface. Elevation data for the cross-profiles on the Tahoe outwash terrace was extracted from the 30 m SRTM DEM.

Three boulder samples for ^{10}Be geochronology were collected from each of the Tahoe and Tioga outwash surfaces. Boulder ages from the Tahoe outwash terrace show a large amount of scatter and did not yield a high- or moderate-confidence depositional age. However, the oldest boulder age (130.8 ± 2.6 ka, Rood et al., 2010) is taken as a minimum depositional age. This minimum age is consistent with our interpretation that the terrace is correlative with other Tahoe outwash surfaces at the Buckeye Creek and Sonora Junction sites. Therefore, we use the average age of these two other, better-dated terraces as the best-estimate age for the Tahoe outwash at Woodfords. We used the individual age PDFs for the Buckeye Creek and Sonora Junction outwash terraces as inputs for an additional Monte Carlo simulation that calculated their average age. We use the resulting histogram as the best-estimate age for the Tahoe terrace at Woodfords of 150 +9/−12 ka (Table 1). Three topographic cross-profiles across the scarp give slip estimates of 59 +21/−9, 42 +20/−10, and 66 + 23/−8 m (Figs. S17–S19) and slip rates of 0.4 +0.2/−0.1, 0.3 ± 0.1, and 0.4 +0.2/−0.1 mm year^{-1}, respectively.

^{10}Be ages from the Tioga outwash terrace indicate deposition at 20.7 ± 1.1 ka (n = 3) (Table 1), whereas survey data suggest slip magnitudes of 10 +5/−2 and 9 +4/−1 m (Figs. S20–S21) and slip rates of 0.5 +0.2/−0.1 and 0.4 +0.2/−0.1 mm year^{-1}. The interval slip rate between the Tahoe and Tioga outwash terraces is 0.4 ± 0.1 mm year^{-1} (Table 2). As found at our other sites, these data permit that, within resolution, slip rates were relatively steady over ~20 ky and ~150 ky timescales across the southern Genoa fault.

4. Discussion

4.1. Resolution of fault slip rates

Our results include: 1) 115 new dates, of which 57 samples are discussed here (Table S2) on landforms spanning from ~20 ka to ~150 ka; 2) quantification of the magnitude of fault offsets at multiple sites along the eastern Sierra Nevada fault system; and 3) improved estimates of uncertainties related to the age, magnitude, and rates of faulting. As a consequence, we have generated a fairly dense array of slip rates over the past 150 ky, spanning both the last and the penultimate glaciations. Our ^{10}Be ages (Table 1) define tightly clustered ages of boulders on individual surfaces that, when considered as a group, yield age uncertainties typically <10% (setting a lower bound on the rate differences we define). The ages of glacial deposits along the eastern Sierra Nevada (Rood et al., 2010) and elsewhere in the Basin and Range demonstrates that events of moraine or terrace abandonment are climatically controlled and tend to be regionally similar in age (Bull, 1991). When compared to alluvial fans, e.g., Benn et al. (2006), glacial deposits in the western Great Basin are especially well suited to slip-rate studies utilizing surface exposure dating, because their similar age, relatively rapid deposition, and minimal inheritance, e.g., Schaefer et al. (2009), permits correlation of geomorphic surfaces and quantification of slip rates at multiple sites with relatively high confidence. Hence, we can go beyond individual well-dated sites to collect data on multiple offsets of the same marker, enabling development of a regional pattern of fault slip.

We intentionally focused on field sites where slip rates are modest (generally <1 mm year^{-1}). On rapidly moving faults, uncertainties typically limit the resolution with which one can discriminate among geomorphic displacement rates, e.g., Behr et al. (2010). Moreover, we chose to study normal fault scarps that can be readily surveyed, and do not suffer from ambiguous offsets that are common with strike-slip faults, specifically with offset alluvial fans and river terraces (Cowgill, 2007; Van der Woerd et al., 2006). At sites such as ours, the use of multiple displaced markers with high-resolution dates permits an improved and robust discrimination of fault slip rates through time and space.

4.2. Temporal slip rate variations

As borne out by every site where offset features of two different ages can be compared, our data permit that, at any given site, slip rates are relatively steady over the timescales examined. Over the last ~20 ky and ~150 ky, mean slip rates are 0.3 ± 0.1 mm year^{-1} at the Buckeye Creek and Sonora Junction sites and 0.4 +0.3/−0.1 mm year^{-1} at Woodfords, and have probably not varied by more than a factor of two over time spans equal to half of the total time interval. Consequently, we deduce that, over numerous seismic cycles, the mean rate of strain accumulation and release on these normal faults is relatively steady over ~20 ky and ~150 ky timescales. Such rates give a useful constraint on the seismic hazard for these individual faults. In addition, these rates provide a valuable baseline for comparison to decadal rates that are derived from geodetic data. For example, when the strain rate between earthquakes is non-linear owing to viscoelastic earthquake processes, geodetic rates early in a seismic cycle (Friedrich et al., 2003) will likely be greater than the long-term average rate (post-seismic rate), whereas late in a seismic cycle, they can be less than the average rate (late interseismic rate). Thus, our geomorphic slip rates can be compared to geodetic rates on these individual faults, and the near-term seismic hazard could potentially be improved by estimating where the fault is in its own cycle.

Rates and patterns fault slip rates over timescales of 10–100 ky provide insight into the timescales of important fault processes, e.g., changes in stress and variable strain accumulation. For example, it was suggested by Bellier and Zoback (1995) that local stress can vary on 10^5 year timescales, and data from the Himalaya suggest stress changes at seasonal time scales (Bettinelli et al., 2008). Changes in stress might explain the variable loading patterns inferred for some faults in the ECSZ-WLB, e.g., Oskin and Iriondo (2004). Some studies provide evidence for different slip rates through middle and the late Quaternary time (50% lower in late Pleistocene versus middle Pleistocene in the northern White Mountains; Lee et al., 2009), as well as coordinated slip rate variations among neighboring faults, e.g. White Mountain fault, Kirby et al. (2006). Slip rate variations similar to those in the northern White Mountains are observed on distributed normal faults in the Volcanic Tablelands of northern Owens Valley (Sheehan, 2007). However, we observe no evidence for such temporal variations in fault slip rates on faults of the central SNFFZ. We interpret this steadiness to indicate that effects of earthquake clustering, local changes in stress, and variable strain accumulation are not affecting slip rate patterns at timescales of ~20 ky and ~150 ky on these individual normal faults. Therefore, these new rates provide a simplified view of patterns in regional fault behavior.

4.3. Spatially variable slip rates

Our data suggest spatially variable slip rates over the past 20 ky along strike of the central SNFFZ. Slip rates differ by at least a factor of three between the northern Mono Basin (1.3 +0.6/−0.3 mm year^{-1} at Lundy Canyon site) and the Bridgeport Basin (0.3 ± 0.1 mm year^{-1} at Buckeye Creek site) ~20 km to the north. This spatial heterogeneity of slip rates along strike could be interpreted in several ways, including temporal clustering of fault slip in the Mono Basin. Given that strain accumulation and release rates observed on other normal

faults of the central SNFFZ do not change by more than a factor of two over ~20 ky and ~150 ky timescales, however, we think that it is more likely that the striking 3–5-fold increase in slip rate observed in northern Mono Basin is related to a regional pattern of strain localization acting on timescales of >20 ky. If regional strain accumulation rates are relatively constant over ~20 ky timescales, then along-strike changes in slip rates most likely reflect either interactions among neighboring faults, e.g., Frankel et al. (2007b), or changes in the modes of strain accumulation, e.g., block rotations (Wesnousky, 2005b).

4.4. Spatial slip rate gradients around the Mina Deflection

Because multiple faults or fault segments can interact over short and intermediate timescales, the resultant coordinated spatial patterns of deformation rates and seismicity can provide insight into physical controls on faulting, e.g., Cowie et al. (2000), Peltzer et al. (2001). For example, changes in fault geometry and kinematics could focus slip on one fault or fault system at the expense of interacting faults nearby (Kirby et al., 2008; Oskin et al., 2008).

A synthesis of our fault slip rates with published results in the region provides insights into the modes of fault-related strain accommodation in the ECSZ-WLB (Fig. 6). South of Mono Basin, dextral slip rates decrease northward into the Mina Deflection on the Owen Valley–White Mountain fault zone from 3–4 mm year^{-1} to ~0.5 mm year^{-1} (Kirby et al., 2006, 2008). Likewise, dextral fault slip rates on the Death Valley–Furnace Creek–Fish Lake Valley fault system decrease northward from 4–5 mm year^{-1} to 2–3 mm year^{-1} as they approach the Mina Deflection (Frankel et al., 2007b). However, rates of horizontal extension toward N65°E increase northward along the Fish Lake fault from 0.1–0.3 mm year^{-1} to 0.5–0.7 mm year^{-1} (Ganev et al., 2009). As slip along the Fish Lake Valley fault diminishes at the Mina Deflection, extension rates increase along the SNFFZ to ~0.7 mm year^{-1} in northern Mono Basin (Fig. 6). These spatial patterns suggest that extension is transferred either from faults systems in the east, e.g., Fish Lake Valley fault and Volcanic Tablelands, or from more distributed faulting, such as just south of Big Pine, to more focused faulting at the Sierran range front near the Mina Deflection.

Along strike of the ECSZ-WLB, the character of deformation changes at the Mina Deflection. South of the Mina Deflection, strain is accommodated in a relatively narrow (~25 km wide) zone of NW-striking dextral or oblique strike-slip faults and NNW- or NE-striking normal faults, e.g., Le et al. (2007) and Lee et al. (2009). Extension is distributed across the ECSZ among diffuse normal and oblique faults, e.g., Greene et al. (2007), and focused onto the Fish Lake Valley fault northward (Ganev et al., 2009) (Fig. 6). However, north of the Mina Deflection, deformation spreads into a broad zone (~60 km wide) where faulting is highly partitioned between NNW-striking normal and NW-striking dextral faults (Oldow et al., 2001; Surpless, 2008; Wesnousky, 2005b). Between the SNFFZ and central Walker Lane, extension is distributed across a broad zone of normal fault-bounded basins. Within the Mina Deflection, existing kinematic models suggest that shear is transferred across a right-step in the ECSZ-WLB by left-lateral strike-slip faults that accommodate clockwise vertical axis block rotations, e.g., Wesnousky (2005b). It is unclear how the extensional component of the faulting is accommodated across this transfer zone. Previous workers speculate that extension in this transfer zone is accommodated by diffuse normal faulting (Ganev et al., 2009; Lee et al., 2009; Sheehan, 2007) or by faults to the east of the Mina Deflection (Frankel et al., 2007b). However, we propose that within the Mina Deflection, the NE–SW extension is focused on the SNFFZ. The high slip (>1 mm year^{-1}) in northern Mono Basin accounts for a large percentage of the modern deformation measured across the zone (Bennett et al., 2003) and no other normal faults of significant length exist at this latitude. Furthermore, the voluminous Quaternary volcanism in Long Valley Caldera and Mono Basin may be related to localized extension and high rates of faulting along the SNFFZ (i.e. Bursik and Sieh, 1989) as extension is transferred from the ECSZ. The 3-fold decrease in the slip rate on the SNFFZ northward from Mono Basin is indicative of a change in the character of faulting north of the Mina Deflection as extension is transferred eastward onto normal faults between the Sierra Nevada and WLB.

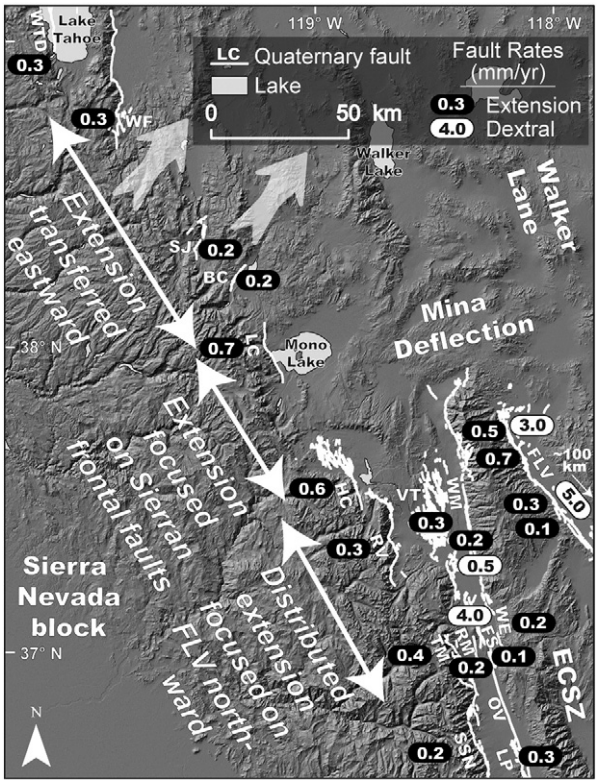

Fig. 6. Extension rates along the transition from the Sierra Nevada to the ECSZ-WLB. LP = Lone Pine fault, SSN = southern SNFFZ, OV = Owens Valley fault, TM = Tinemaha Creek frontal fault, RM = Red Mountain fault, FS = Fish Springs fault, WM = White Mountain fault, VT = Volcanic Tableland, RV = Round Valley fault, HC = Hilton Creek fault, FSV = Fish Springs Valley fault (extensional rates from Ganev et al., 2009 and dextral rates from Frankel et al., 2007b), LC = Lundy Canyon, BC = Buckeye Creek, SJ = Sonora Junction, WF = Woodfords, and WTD = West Tahoe–Dollar Point fault.

5. Conclusions

The combination of numerous new cosmogenic ages on offset moraines and outwash terraces with detailed scarp surveys and Monte Carlo modeling underpin new insights about the evolution of the frontal fault system along the eastern flank of the Sierra Nevada. We deduce that:

(1) Data permits that slip rates across the central SNFFZ have been relatively constant over ~20 ky and ~150 ky timescales. Slip rates have probably not varied by more than a factor of two over time spans equal to half of the total time interval. Over a N–S span of ~80 km, slip rates are 0.3 ± 0.1 mm year^{-1} at the Buckeye Creek and Sonora Junction sites and 0.4 +0.3/–0.1 mm year^{-1} at Woodfords over the last ~20 ky and ~150 ky.

(2) Slip rates are highly variable in space over the last ~20 ky with an especially striking 3–5-fold decrease change across the 20 km between the northern Mono Basin and the neighboring Bridgeport basin. As faults of the ECSZ approach the Mina Deflection, dip-slip rates increase northward along the SNFFZ to 1.3 +0.6/−0.3 mm year^{-1} in northern Mono Basin (Lundy Canyon site), then decrease sharply northward to 0.3 ± 0.1 mm year^{-1} in the Bridgeport Basin.

(3) South of Mono Basin, this northward spatial pattern suggests transfer of extension from faults systems to the east (e.g. Fish Lake Valley fault and Volcanic Tablelands) to the SNFFZ as slip is transferred from the ECSZ to the central WLB at the Mina Deflection. North of Mono Basin, the 3-fold decrease in the slip rate on the SNFFZ northward suggests slip is transferred eastward and distributed among multiple normal faults between the Sierra Nevada and WLB.

(4) High slip rates on faults of the central SNFFZ in and around Mono Basin suggest high seismic hazard in the region, either from more frequent or larger magnitude earthquakes.

Acknowledgements

We thank Lewis Owen and Steve Wesnousky for constructive reviews of the manuscript. Phil Gans and Bodo Bookhagen provided useful comments on an early draft. We also thank Scott Herman, Colin Amos, Steve DeOreo, Willy Amidon, Adam Avakian, Matt Purvance, Alan Ramelli, and Daisy Rood for assistance in the field. We are grateful to Alan Ramelli for providing the total station survey data at Woodfords. Special thanks to Malcolm Clark, Angela Jayko, Doug Clark, Bob Curry, and Burt Slemmons for all their help and insights concerning the Quaternary of the Sierra Nevada. DR is grateful for the mentorship of Tom Brown and Tom Guilderson at the Center for Accelerator Mass Spectrometry at Lawrence Livermore National Laboratory (LLNL) during ^{10}Be measurements. Funding was provided by a LLNL Lawrence Scholar Program (LSP) Fellowship and a GSA Graduate Student Research Grant (to DR). This work was performed under the auspices of the US Department of Energy by Lawrence Livermore National Laboratory under Contract DE-AC52-07NA27344.

Appendix A. Supplementary data

Supplementary data to this article can be found online at doi:10.1016/j.epsl.2010.11.006.

References

Amos, C.B., Burbank, D.W., Nobes, D.C., Read, S.A.L., 2007. Geomorphic constraints on listric thrust faulting: implications for active deformation in the Mackenzie Basin, South Island, New Zealand. J. Geophys. Res. 112 (B3) B03S11.

Anderson, R.S., Repka, J.L., Dick, G.S., 1996. Explicit treatment of inheritance in dating depositional surfaces using in situ ^{10}Be and ^{26}Al. Geology 24 (1), 47–51.

Armin, R.A., John, D.A., 1983. Geologic map of the Freel Peak 15-minute Quadrangle, California and Nevada. Miscellaneous Investigations Series — U. S. Geological Survey Report: I-1424. 1 sheet.

Behr, W.M., Rood, D.H., Fletcher, K.E., Guzman, N., Finkel, R., Hanks, T.C., Hudnut, K.W., Kendrick, K.J., Platt, J.P., Sharp, W.D., Weldon, R., Yule, J.D., 2010. Uncertainties in slip rate estimates for the Mission Creek strand of the southern San Andreas fault at Biskra Palms Oasis, southern California. Geol. Soc. Am. Bull. 122 (9–10), 1360–1377.

Bellier, O., Zoback, M.L., 1995. Recent state of stress change in the Walker Lane zone, western Basin and Range province, United States. Tectonics 14 (3), 564–593.

Benn, D.I., Owen, L.A., Finkel, R.C., Clemmens, S., 2006. Pleistocene lake outburst floods and fan formation along the eastern Sierra Nevada, California: implications for the interpretation of intermontane lacustrine records. Quatern. Sci. Rev. 25 (21–22), 2729–2748.

Bennett, R.A., Wernicke, B.P., Davis, J.L., 1998. Continuous GPS measurements of contemporary deformation across the Northern Basin and Range Province. Geophys. Res. Lett. 25 (4), 563–566.

Bennett, R.A., Wernicke, B.P., Niemi, N.A., Friedrich, A.M., Davis, J.L., 2003. Contemporary strain rates in the northern Basin and Range province from GPS data. Tectonics 22 (2), 1008.

Berry, M.E., 1997. Geomorphic analysis of late Quaternary faulting on Hilton Creek, Round Valley and Coyote warp faults, east-central Sierra Nevada, California, USA. Geomorphology 20 (1–2), 177–195.

Bettinelli, P., Avouac, J., Flouzat, M., Bollinger, L., Ramillien, G., Rajaure, S., Sapkota, S., 2008. Seasonal variations of seismicity and geodetic strain in the Himalaya induced by surface hydrology. Earth Planet. Sci. Lett. 266, 332–344.

Brothers, D.S., Kent, G.M., Driscoll, N.W., Smith, S.B., Karlin, R., Dingler, J.A., Harding, A.J., Seitz, G.G., Babcock, J.M., 2009. New constraints on deformation, slip rate, and timing of the most recent earthquake on the West Tahoe–Dollar Point Fault, Lake Tahoe Basin, California. Bull. Seismol. Soc. Am. 99 (2A), 499–519.

Bull, W.B., 1991. Geomorphic Responses to Climatic Change. Oxford Univ. Press, New York, NY, United States (USA).

Bursik, M., Sieh, K.E., 1989. Range front faulting and volcanism in the Mono basin, eastern California. J. Geophys. Res. 94 (B11) 15,587–15,609.

Bursik, M. I. 1989. Late Quaternary volcano-tectonic evolution of the Mono Basin, eastern California. Unpublished doctoral thesis, California Institute of Technology.

Cashman, P.H., Fontaine, S.A., 2000. Strain partitioning in the northern Walker Lane, western Nevada and northeastern California. Tectonophysics 326 (1–2), 111–130.

Chevalier, M.L., Ryerson, F.J., Tapponnier, P., Finkel, R.C., Van Der Woerd, J., Haibing, L., Qing, L., 2005. Slip-rate measurements on the Karakorum Fault may imply secular variations in fault motion. Science 307 (5708), 411–414.

Clark, D., Gillespie, A.R., Clark, M.M., Burke, B., 2003. Mountain Glaciations of the Sierra Nevada. Desert Research Institute, Reno, NV, United States (USA).

Clark, M. 1967. Pleistocene glaciation of the drainage of the West Walker River, Sierra Nevada, California. Unpublished doctoral thesis, Stanford University.

Cowgill, E., 2007. Impact of riser reconstructions on estimation of secular variation in rates of strike-slip faulting: revisiting the Cherchen River site along the Altyn Tagh Fault, NW China. Earth Planet. Sci. Lett. 254 (3–4), 239–255.

Cowgill, E., Gold, R.D., Xuanhua, C., Xiao-Feng, W., Arrowsmith, J.R., Southon, J., 2009. Low Quaternary slip rate reconciles geodetic and geologic rates along the Altyn Tagh fault, northwestern Tibet. Geology 37 (7), 647–650.

Cowie, P.A., Gupta, S., Dawers, N.H., 2000. Implications of fault array evolution for synrift depocentre development: insights from a numerical fault growth model. Basin Res. 12 (3/4), 241.

Davis, K., Burbank, D.W., Fisher, D., Wallace, S., Nobes, D., 2005. Thrust-fault growth and segment linkage in the active Ostler fault zone, New Zealand. J. Struct. Geol. 27 (8), 1528–1546.

DeCelles, P.G., Robinson, D.M., Zandt, G., 2002. Implications of shortening in the Himalayan fold-thrust belt for uplift of the Tibetan Plateau. Tectonics 21 (6), 1062.

DeMets, C., Dixon, T.H., 1999. New kinematic models for Pacific-North America motion from 3 Ma to present, I: evidence for steady motion and biases in the NUVEL-1A Model. Geophys. Res. Lett. 26 (13), 1921–1924.

Dixon, T., Farina, F., DeMets, C., Suarez Vidal, F., 2000. New kinematic models for Pacific-North America Motion from 3 Ma to Present, II: evidence for a "Baja California Shear Zone". Geophys. Res. Lett. 27 (23), 3961–3964.

Dixon, T.H., Norabuena, E., Hotaling, L., 2003. Paleoseismology and Global Positioning System: earthquake-cycle effects and geodetic versus geologic fault slip rates in the Eastern California shear zone. Geology 31 (1), 55–58.

Dixon, T.H., Robaudo, S., Lee, J., Reheis, M.C., 1995. Constraints on present-day Basin and Range deformation from space geodesy. Tectonics 14 (4), 755–772.

Dokka, R.K., Travis, C.J., 1990. Role of the Eastern California Shear Zone in accommodating Pacific-North American Plate motion. Geophys. Res. Lett. 17 (9), 1323–1326.

Dolan, J.F., Bowman, D.D., Sammis, C.G., 2007. Long-range and long-term fault interactions in Southern California. Geology 35 (9), 855–858.

Eddington, P.K., Smith, R.B., Renggli, C., 1987. Kinematics of Basin and Range intraplate extension. Geol. Soc. Spec.Publ. 28, 371–392.

Frankel, K.L., Brantley, K.S., Dolan, J.F., Finkel, R.C., Klinger, R.E., Knott, J.R., Machette, M.N., Owen, L.A., Phillips, F.M., Slate, J.L., Wernicke, B.P., 2007a. Cosmogenic ^{10}Be and ^{36}Cl geochronology of offset alluvial fans along the northern Death Valley fault zone: implications for transient strain in the eastern California shear zone. J. Geophys. Res. 112 (B6), B06407.

Frankel, K.L., Dolan, J.F., Finkel, R.C., Owen, L.A., Hoeft, J.S., 2007b. Spatial variations in slip rate along the Death Valley–Fish Lake Valley fault system determined from LiDAR topographic data and cosmogenic ^{10}Be geochronology. Geophys. Res. Lett. 34 (18), L18303.

Friedrich, A.M., Wernicke, B.P., Niemi, N.A., Bennett, R.A., Davis, J.L., 2003. Comparison of geodetic and geologic data from the Wasatch region, Utah, and implications for the spectral character of Earth deformation at periods of 10 to 10 million years. J. Geophys. Res. 108 (B4), 2199.

Ganev, P.N., Dolan, J.F., Frankel, K.L., Finkel, R.C., 2009. Rates of extension along the Fish Lake Valley fault and transtensional deformation in the Eastern California shear zone–Walker Lane belt. Lithosphere 2 (1), 33–49.

Glazner, A.F., Lee, J., Bartley, J.M., Coleman, D.S., Kylander-Clark, A., Green, D.C., Le, K., 2005. Large dextral offset across Owens Valley, California from 148 Ma to 1872 A.D. In: Stevens, C., Cooper, J. (Eds.), Western Great Basin Geology, The Pacific Section Society of Sedimentary Geology, vol. 99. pp. 1–35.

Gosse, J.C., Phillips, F.M., 2001. Terrestrial in situ cosmogenic nuclides: theory and application. Quatern. Sci. Rev. 20 (14), 1475–1560.

Greene, D., Kirby, E., Dawers, N., Phillips, F., McGee, S., Burbank, D., 2007. Quantifying accommodation of active strain along distributed fault arrays in Owens Valley, California. Geological Society of America Abstracts with Programs 39 (6), 441.

Hammond, W.C., Thatcher, W., 2004. Contemporary tectonic deformation of the Basin and Range province, western United States: 10 years of observation with the Global Positioning System. J. Geophys. Res. 109 (B8), B08403.

Hampel, A., Hetzel, R., 2008. Slip reversals on active normal faults related to the inflation and deflation of magma chambers: numerical modeling with application to the Yellowstone–Teton region. Geophys. Res. Lett. 35 (7), L07301.

Hampel, A., Hetzel, R., Densmore, A.L., 2007. Postglacial slip-rate increase on the Teton normal fault, northern Basin and Range Province, caused by melting of the Yellowstone ice cap and deglaciation of the Teton Range? Geology 35 (12), 1107–1110.

Hampel, A., Hetzel, R., Maniatis, G., Karow, T., 2009. Three-dimensional numerical modeling of slip rate variations on normal and thrust fault arrays during ice cap growth and melting. J. Geophys. Res. 114 (B8), B08406.

Hetzel, R., Hampel, A., 2005. Slip rate variations on normal faults during glacial–interglacial changes in surface loads. Nature 435 (7038), 81–84.

Kent, G.M., Babcock, J.M., Driscoll, N.W., Harding, A.J., Dingler, J.A., Seitz, G.G., Gardner, J.V., Mayer, L.A., Goldman, C.R., Heyvaert, A.C., Richards, R.C., Karlin, R., Morgan, C.W.,

Gayes, P.T., Owen, L.A., 2005. 60 k.y. record of extension across the western boundary of the Basin and Range province: estimate of slip rates from offset shoreline terraces and a catastrophic slide beneath Lake Tahoe. Geology 33 (5), 365–368.

Kessler, M.A., Anderson, R.S., Stock, G.M., 2006. Modeling topographic and climatic control of east–west asymmetry in Sierra Nevada glacier length during the Last Glacial Maximum. J. Geophys. Res. 111 (F2), F02002.

Kirby, E., Anandakrishnan, S., Phillips, F., Marrero, S., 2008. Late Pleistocene slip rate along the Owens Valley fault, eastern California. Geophys. Res. Lett. 35 (1), L01304.

Kirby, E., Burbank, D.W., Reheis, M., Phillips, F., 2006. Temporal variations in slip rate of the White Mountain Fault Zone, Eastern California. Earth Planet. Sci. Lett. 248 (1–2), 168–185.

Le, K., Lee, J., Owen, L.A., Finkel, R., 2007. Late Quaternary slip rates along the Sierra Nevada frontal fault zone, California: slip partitioning across the western margin of the Eastern California Shear Zone-Basin and Range Province. Geol. Soc. Am. Bull. 119 (1–2), 240–256.

Lee, J., Garwood, J., Stockli, D.F., Gosse, J., 2009. Quaternary faulting in Queen Valley, California–Nevada: implications for kinematics of fault-slip transfer in the eastern California shear zone–Walker Lane belt. Geol. Soc. Am. Bull. 121 (3–4), 599–614.

Lee, J., Spencer, J., Owen, L., 2001. Holocene slip rates along the Owens Valley fault, California: implications for the recent evolution of the Eastern California Shear Zone. Geology 29 (9), 819–822.

Lubetkin, L.K.C., Clark, M.M., 1988. Late Quaternary activity along the Lone Pine fault, eastern California. Geol. Soc. Am. Bull. 100 (5), 755–766.

Martel, S.J., Harrison, T.M., Gillespie, A.R., 1987. Late Quaternary vertical displacement rate across the Fish Springs fault, Owens Valley fault zone, California. Quatern. Res. 27 (2), 113–129.

Oldow, J.S., 2003. Active transtensional boundary zone between the western Great Basin and Sierra Nevada block, western U.S. Cordillera. Geology 31 (12), 1033–1036.

Oldow, J.S., Aiken, C.L.V., Hare, J.L., Ferguson, J.F., Hardyman, R.F., 2001. Active displacement transfer and differential block motion within the central Walker Lane, western Great Basin. Geology 29 (1), 19–22.

Oskin, M., Iriondo, A., 2004. Large-magnitude transient strain accumulation on the Blackwater fault, Eastern California shear zone. Geology 32 (4), 313–316.

Oskin, M., Perg, L., Blumentritt, D., Mukhopadhyay, S., Iriondo, A., 2007. Slip rate of the Calico fault: implications for geologic versus geodetic rate discrepancy in the Eastern California Shear Zone. J. Geophys. Res. 112 (B3), B03402.

Oskin, M., Perg, L., Shelef, E., Strane, M., Gurney, E., Singer, B., Zhang, X., 2008. Elevated shear zone loading rate during an earthquake cluster in eastern California. Geology 36 (6), 507–510.

Peltzer, G., Crampe, F., Hensley, S., Rosen, P., 2001. Transient strain accumulation and fault interaction in the Eastern California shear zone. Geology 29 (11), 975–978.

Petronis, M.S., Geissman, J.W., Oldow, J.S., McIntosh, W.C., 2002. Paleomagnetic and 40Ar/39Ar geochronologic data bearing on the structural evolution of the Silver Peak extensional complex, west-central Nevada. Geol. Soc. Am. Bull. 114 (9), 1108–1130.

Ramelli, A.R., Bell, J.W., dePolo, C.M., Yount, J.C., 1999. Large-magnitude, late Holocene earthquakes on the Genoa Fault, west-central Nevada and eastern California. Bull. Seismol. Soc. Am. 89 (6), 1458–1472.

Rockwell, T.K., Lindvall, S., Herzberg, M., Murbach, D., Dawson, T., Berger, G., 2000. Paleoseismology of the Johnson Valley, Kickapoo, and Homestead Valley Faults: clustering of Earthquakes in the Eastern California Shear Zone. Bull. Seismol. Soc. Am. 90 (5), 1200–1236.

Rood, D.H., Burbank, D.W., Finkel, R., 2010. Chronology of glaciations in the Sierra Nevada, California, from ^{10}Be surface exposure dating. Quatern. Sci. Rev. doi:10.1016/j.quascirev.2010.12.001.

Sauber, J., Thatcher, W., Solomon, S.C., Lisowski, M., 1994. Geodetic slip rate for the eastern california shear zone and the recurrence time of mojave desert earthquakes. Nature (London) 367 (6460), 264–266.

Savage, J.C., Gan, W., Svarc, J.L., 2001. Strain accumulation and rotation in the eastern california shear zone. J. Geophys. Res. 106 (B10) 21,995–22,007.

Savage, J.C., Lisowski, M., Prescott, W.H., 1990. An apparent shear zone trending north-northwest across the Mojave Desert into Owens Valley, eastern California. Geophys. Res. Lett. 17 (12), 2113–2116.

Schaefer, J.M., Denton, G.H., Kaplan, M., Putnam, A., Finkel, R.C., Barrell, D.J.A., Andersen, B.G., Schwartz, R., Mackintosh, A., Chinn, T., Schluchter, C., 2009. High-frequency Holocene glacier fluctuations in New Zealand differ from the Northern Signature. Science 324 (5927), 622–625.

Schweickert, R.A., Lahren, M.M., Smith, K.D., Howle, J.F., Ichinose, G., 2004. Transtensional deformation in the Lake Tahoe region, California and Nevada, USA. Tectonophysics 392 (1–4), 303–323.

Sharp, R.P., 1972. Pleistocene glaciation, Bridgeport Basin, California. Geol. Soc. Am. Bull. 83 (8), 2233–2260.

Sheehan, T. P. 2007. Evolution of Neogene fault populations in northern Owens Valley, California and implications for the eastern California shear zone. Unpublished doctoral thesis, Tulane University.

Surpless, B., 2008. Modern strain localization in the central Walker Lane, western United States: Implications for the evolution of intraplate deformation in transtensional settings. Tectonophysics 457 (3–4), 239–253.

Thatcher, W., Foulger, G.R., Julian, B.R., Svarc, J., Quilty, E., Bawden, G.W., 1999. Present-day deformation across the Basin and Range Province, Western United States. Science 283 (5408), 1714–1718.

Thompson, S.C., Weldon, R.J., Rubin, C.M., Abdrakhmatov, K., Molnar, P., Berger, G.W., 2002. Late Quaternary slip rates across the central Tien Shan, Kyrgyzstan, central Asia. J. Geophys. Res. 107 (B9), 2203.

Unruh, J., Humphrey, J., Barron, A., 2003. Transtensional model for the Sierra Nevada frontal fault system, eastern California. Geology 31 (4), 327–330.

Van der Woerd, J., Klinger, Y., Sieh, K., Tapponnier, P., Ryerson, F.J., Mériaux, A.-S., 2006. Long-term slip rate of the southern San Andreas Fault from ^{10}Be–^{26}Al surface exposure dating of an offset alluvial fan. J. Geophys. Res. 111 (B4), B04407.

Wakabayashi, J., Sawyer, T.L., 2001. Stream incision, tectonics, uplift, and evolution of topography of the Sierra Nevada, California. J. Geol. 109 (5), 539–562.

Wallace, R.E., 1987. Grouping and migration of surface faulting and variations in slip rates on faults in the Great Basin province. Bull. Seismol. Soc. Am. 77 (3), 868–876.

Wang, Q., Zhang, P.-Z., Freymueller, J.T., Bilham, R., Larson, K.M., Lai, X., You, X., Niu, Z., Wu, J., Li, Y., Liu, J., Yang, Z., Chen, Q., 2001. Present-day crustal deformation in China constrained by Global Positioning System measurements. Science 294 (5542), 574–577.

Weldon, R.J., Fumal, T.E., Biasi, G.P., Scharer, K.M., 2004. Implications from a long window of observation; the San Andreas Fault at Wrightwood, California. Seismol. Res. Lett. 75 (2), 244.

Wesnousky, S.G., 2005a. Active faulting in the Walker Lane. Tectonics 24 (3) TC3009.

Wesnousky, S.G., 2005b. The San Andreas and Walker Lane fault systems, western North America: transpression, transtension, cumulative slip and the structural evolution of a major transform plate boundary. J. Struct. Geol. 27 (8), 1505–1512.

Zechar, J.D., Frankel, K.L., 2009. Incorporating and reporting uncertainties in fault slip rates. J. Geophys. Res. 114 (B12), B12407.

Zehfuss, P.H., Bierman, P.R., Gillespie, A.R., Burke, R.M., Caffee, M.W., 2001. Slip rates on the Fish Springs fault, Owens Valley, California, deduced from cosmogenic ^{10}Be and ^{26}Al and soil development on fan surfaces. Geol. Soc. Am. Bull. 113 (2), 241–255.